ELSEVIER

Polymer 44 (2003) 2351–2362

polymer

www.elsevier.com/locate/polymer

Rigid-particle toughening of glassy polymers

David A. Norman, Richard E. Robertson*

Department of Materials Science and Engineering, The University of Michigan, 2014 H. H. Dow Building, 2300 Haywood Street, Ann Arbor, MI 48109-2136, USA

Received 4 October 2002; received in revised form 13 January 2003; accepted 15 January 2003

Abstract

The nature of the toughening of glassy polymers by rigid particles was investigated by using aligned assemblages of spherical glass particles. The particles were aligned by an electric field in a photopolymerizable monomer, which was polymerized while the field was still being applied. These materials were fractured with the aligned particle strings in three orientations with respect to the crack plane and propagation direction. The fracture toughness and fracture energy of these and of random arrangements of particles (formed without the electric field) were all higher than of the matrix alone. The increases were compared with predictions from processes on or in the immediate vicinity of the fracture plane and from those away from the fracture plane. The increases were inconsistent with those predicted by on-fracture plane processes as represented by crack pinning and bowing. But the increases did correlate with the size of the process zones, which could extend more than 100 μm away from the fracture plane. Detailed calculations showed that the increase in fracture energy arose almost completely from off-fracture plane processes of particle-matrix debonding and the accompanying local inelastic deformation of the matrix around the particles.

Keywords: Fracture mechanics; Debonding; Yield

1. Introduction

Rigid, inorganic particles are added to polymers for a number of reasons, which include property modification, processing aids, and cost reduction [1]. Although many thermoplastics are embrittled by the addition of rigid particles, the fracture toughness of glassy polymers, especially thermosets, has been improved by such fillers, even though the particles used can have a significantly lower fracture energy than the polymers they toughen. The fracture energies of filled thermosets have been found to be ca. 2–4 times that of the matrix alone, with the maximum typically occurring at a particle volume fraction between 0.1 and 0.4 [1–12]. The fracture energy of a glass bead-filled polystyrene was 1.8 times that of the neat polymer at a particle volume fraction of about 0.05 [13]. Although this phenomenon, known as rigid-particle toughening, has been studied for more than 30 years, an understanding of its origins has been lacking.

The explanations offered for rigid-particle toughening can be grouped into two categories: processes that occur on or in the immediate vicinity of the fracture plane and those off or away from the fracture plane. The principal on-fracture plane process toughens by having the crack front interact with second-phase particles, which by pinning the crack front, force it to bow out between the particles during propagation. Lange [14] was the first to propose a relationship between crack bowing and rigid-particle toughening, and Evans [15] and Green [16] further developed this into a crack bowing theory. The theory relates toughening to the geometry of the system, which includes the separation between the particles that are within the fracture plane, particle size, and the distance the bowed crack must propagate before breaking free of the particles. Off-fracture plane processes toughen by the occurrence of damage in a volume away from the crack tip. The damage includes particle-matrix debonding [11,12,17,18] and matrix yielding [12,18], and may extend 100 μm or more on either side of the fracture plane [19,20].

Toughening is commonly thought to involve both on- and off-fracture plane processes to some extent, though crack pinning and bowing is often thought to be the more important mechanism [2,4–10,21–23]. Most comparisons

* Corresponding author. Tel.: +1-734-763-9867; fax: +1-734-763-4788.
E-mail address: rer@umich.edu (R.E. Robertson).

0032-3861/03/$ - see front matter © 2003 Elsevier Science Ltd. All rights reserved.
doi:10.1016/S0032-3861(03)00084-3

of the crack bowing theory of Evans [15] and Green [16] with experimental data have found reasonable agreement [8–10,20,22]. But off-fracture plane processes are thought by others to be dominant [11,17–20]. The problem is that the relative contributions of the two types of processes have not been able to be determined from the available experimental data up to now. For example, Lee and Yee showed the importance of off-fracture plane processes for toughening a glass bead-filled epoxy, yet they still found the crack bowing theory to give an adequate fit to their data [20].

In an attempt to assess the relative importance of on- and off-fracture plane processes, we investigated the fracture behavior of composites with spatially arranged particles. Ordered composites were prepared by suspending particles in a non-conductive monomer, aligning the particles with an electric field, and polymerizing the monomer to capture the aligned microstructure. On-fracture plane processes, as described by crack bowing theory, predict toughening to depend on the separation of particles within the fracture plane, and off-fracture plane processes are expected to depend on the arrangement of particles away from the fracture plane [19]. Experiments were able to be performed on composite specimens that were identical except that the particles were either randomly dispersed or aligned into strings. The aligning process altered the particle arrangement within or away from the fracture plane without changing the particle density in the fracture plane.

2. Experimental

2.1. Materials

A mixture of two photopolymerizable monomers were used for the matrix phase. These were urethane dimethacrylate (UDMA) and 1,6-hexanediol dimethacrylate (HDDMA). The monomers were mixed in a 9:1 ratio by weight of UDMA to HDDMA to achieve a viscosity of ca. 2.5 Pa s [24]. Camphorquinone (0.3 wt%) and *N*,*N*-dimethylaminoethyl methacrylate (0.2 wt%) were added as a light-activated initiator and accelerator, respectively. Glass spheres (Spheriglass 4000A, Potters Industries Inc.) were used as the reinforcement. The glass spheres had a mean particle diameter of 20 μm with a broad size distribution (<5 μm, 10%; <18 μm, 50%; <45 μm, 90%). The particles were used as received and had no surface treatment such as a silane coating. Observation by scanning electron microscopy showed the surface of the particles to be clean, which should provide a moderately strong bond to the matrix in the absence of moisture.

2.2. Specimen preparation

Aligned specimens were prepared using the following procedure. Glass spheres and monomers were mixed by hand with an agate mortar and pestle. Once mixed, the suspension was heated to ca. 75 °C to allow entrapped air to rise to the surface. After cooling, the suspension was carefully poured into a cell similar to that in Fig. 1. These cells were constructed from a glass slide (75×50 mm^2), poly(methyl methacrylate) (PMMA) spacers, aluminum electrodes, blocks of a polymeric, open-cell foam, and a PMMA cover. The aluminum electrodes were adhesively bonded to the PMMA spacers, and the spacers and foam blocks were bonded to the glass slide, leaving a rectangular cavity. The PMMA spacers were oriented such that the electrodes faced each other on the inside of the cavity. Depending on the desired particle alignment, the electrodes were positioned on either the sides or ends of the specimen. The spacers determined the height of the cavity, which was enclosed by the PMMA cover. Specimens were exposed to an AC electric field of 0.43 kV/mm, which was generated by a Transco 4B15N3-02 transformer (15 kV at 60 Hz) coupled with a Staco 3PN1010 variable autotransformer. After exposure to the field for 1 min, the monomers were photopolymerized using blue light as the specimen remained under the field; this initial cure was performed with a Dentsply Prismetics Lite hand-held light source for approximately 5 min. The foam blocks minimized residual stresses or voids arising from specimen shrinkage during cure. (The foam left an irregular surface finish, which was later ground away.) The initial light cure was followed by light and thermal post-cure steps to ensure that all specimens reached a similar state of cure. The specimens were first exposed to a more powerful light source (Dentsply Triad II) for 20 min. The specimens were then heated to 175 °C under a vacuum for 2 h. This temperature was chosen based on differential scanning calorimetry of the

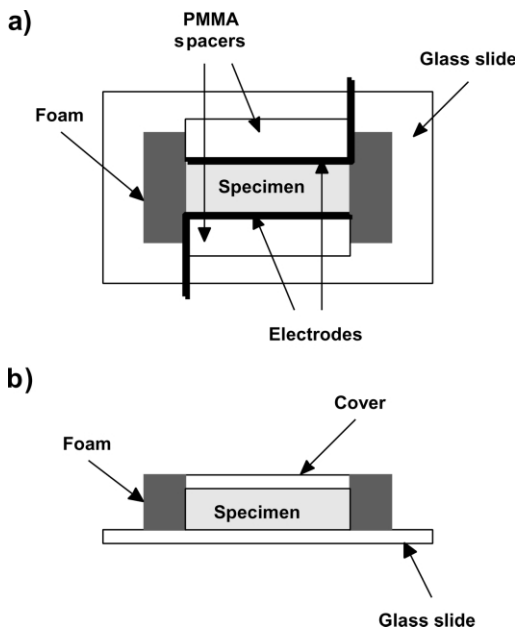

Fig. 1. Schematic of a cell for preparation of aligned specimens shown in (a) plan and (b) side views.

resin system, which showed that thermal cure was complete ca. 160 °C.

Non-aligned specimens were prepared using the same procedure, except they were not subjected to the electric field prior to polymerization.

In addition to the unfilled resin, specimens were prepared with particle concentrations of 10, 20, and 30 vol% for each particle arrangement.

2.3. Microscopy

Observations of fracture surfaces and sections of specimens were made with scanning electron and optical microscopy. Scanning electron microscopy was performed on fracture surfaces using a Philips XL30FEG microscope. Specimens were first coated with a thin film of carbon to make them electrically conductive. Optical microscopy was performed using an Olympus BH-2 polarizing microscope. Specimens sections, having thicknesses of 1–2 mm, were obtained with a Buehler Isomet low-speed diamond saw, and both sides of the sections were polished. Observations were made using transmitted light.

To observe fracture and flexural specimens under load, a fixture was fabricated to fit the stage of the optical microscope. Fracture specimens were wedge-loaded, and flexural specimens were loaded in three-point bending. Specimen geometry was similar to that described for mechanical testing, except for the thickness being 1–2 mm.

2.4. Mechanical testing

The fracture toughness, flexural modulus, and onset of inelastic deformation were measured. Fracture toughness was obtained from single-edge-notched specimens loaded in three-point bending. Fracture specimens were notched using a thin saw blade and pre-cracked at the end of the notch with a razor blade. The fracture toughness, K_{Ic}, was calculated from [25]

$$K_{Ic} = \frac{P_c S}{W H^{3/2}} f(a/H) \quad (1)$$

where P_c is the load at fracture, S the span between support pins (30.3 mm), W the specimen width, H the specimen height, and a the crack length. Typical dimensions of the fracture specimens were $35 \times 6 \times 14\ mm^3$ ($L \times W \times H$), and the ratio a/H was maintained at ca. 0.5 for all specimens, giving a value of ca. 2.7 for $f(a/H)$. Certain specimens were made with slightly smaller dimensions because the depth of the photopolymerization was limited.

Fracture toughness results were also converted to fracture energy, G_{ic}. For the non-aligned specimens, fracture energy was calculated from [26]

$$G_{ic} = \frac{K_{Ic}^2}{E}(1 - \nu^2) \quad (2)$$

where E is Young's modulus and ν Poisson's ratio. For the aligned specimens, fracture energy was calculated using orthotropic fracture mechanics [27] because alignment caused the elastic behavior to become anisotropic, although anisotropy of Poisson's ratio was neglected.

Young's modulus was estimated by the flexural modulus. The flexural modulus was obtained with unnotched specimens flexed in three-point bending and calculated from

$$E = \frac{S^3}{4WH^3} \frac{\Delta P}{\Delta D} \quad (3)$$

where $\Delta P/\Delta D$ is the slope of the load versus displacement curve within the linear region. The dimensions of the flexural specimens were nominally $35 \times 14 \times 3\ mm^3$ ($L \times W \times H$), and S was 30.3 mm. Poisson's ratio was estimated using the rule of mixture

$$\nu_c = \nu_f V_f + \nu_m(1 - V_f) \quad (4)$$

where V_f is the filler volume fraction, and the subscripts c, m, and f refer to composite, matrix and filler. Values of 0.22 and 0.38 were used for Poisson's ratio of the filler and matrix, respectively.

The onset of inelastic deformation was also obtained from unnotched specimens flexed in three-point bending. The onset, σ_{ii}, corresponded to the deviation from linearity of the load versus displacement curve. Because the deviation from linearity was gradual, σ_{ii} was defined by an offset strain of 0.1%. This offset value was chosen because it could be measured reproducibly and was below the strain at which most specimens failed in flexure.

All mechanical tests were performed on a 4502 Instron with a crosshead speed of 0.5 mm/min. The fracture and flexural results presented are the average of six equivalent specimens.

Specimen dimensions used in the above equations were the average of four measurements.

3. Results

3.1. Microstructures

Typical microstructures visible on fracture surfaces of specimens with 20 vol% glass spheres are shown in Fig. 2. For the non-aligned composite (Fig. 2(a)), the particles were randomly distributed across the fracture surface. For the aligned composite, strings of particles along the electric field axis are seen (Fig. 2(b)). The length of the strings varied widely over the range 50–275 μm and increased with particle concentration. The average lengths were ca. 90, 130, and 140 μm for particle concentrations of 10, 20, and 30 vol%, respectively. The average string length at 20 vol% corresponds roughly to six average-sized particles (ca. 20 μm diameter). However, strings frequently contained more than six particles because smaller particles filled the gaps between larger ones or congregated at string ends. The width of the strings was roughly equal to that of a

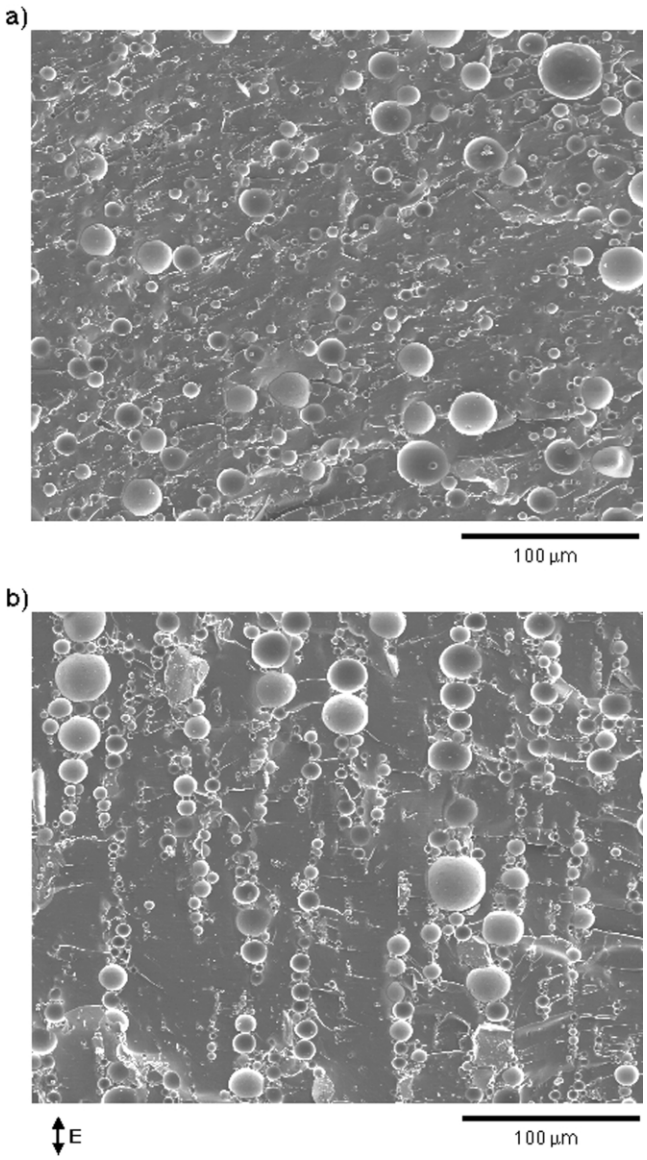

Fig. 2. Fracture surfaces of (a) random and (b) aligned specimens, showing typical particle arrangements. Particle concentration was 20 vol% for both micrographs.

single average-sized particle, although several small particles occasionally spanned this width.

3.2. Fracture toughness and fracture energy

For the fracture experiments, three different particle orientations were investigated (Fig. 3), in addition to randomly dispersed particles. These orientations were given names to describe the relationship between the alignment axis and the crack plane and propagation direction. With the strings perpendicular to the fracture plane (Fig. 3(a)), the specimen was termed 'normal-aligned.' With the particulate strings in the fracture plane and aligned with the propagation direction (Fig. 3(b)), the specimen was termed 'in-plane parallel-aligned.' And with

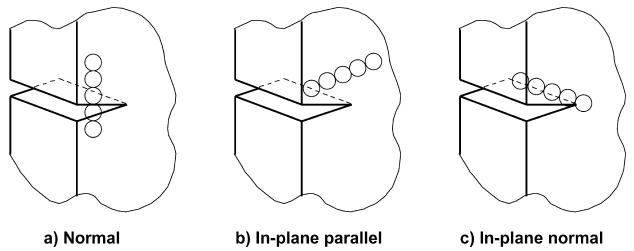

Fig. 3. The three aligned-particle orientations investigated: (a) normal-aligned, (b) in-plane parallel-aligned, and (c) in-plane normal-aligned.

the particulate strings in the fracture plane and aligned normal to the propagation direction (Fig. 3(c)), the specimen was termed 'in-plane normal-aligned.'

The fracture toughness, K_{Ic}, and its dependence on particle concentration and arrangement are shown in Fig. 4. Although the only particle concentrations studied were 0, 10, 20, and 30 vol%, the data in Fig. 4 have been shifted about these concentrations to avoid overlap of the fracture toughness and error bars for the different particle arrangements. The fracture toughness of the neat resin was 1.1 MPa $m^{1/2}$. With non-aligned particles, the average fracture toughness increased ca. 1.8 times from 0 and 20 vol% glass spheres and appeared to reach a plateau above 20 vol%. At 10 vol% glass spheres, all particle arrangements had about the same fracture toughness. At 20 and 30 vol%, the normal-aligned specimens were tougher than the non-aligned, the in-plane parallel-aligned specimens had about the same toughness as the non-aligned, and at 20 vol% glass spheres, the in-plane normal specimens were less tough than the non-aligned. In-plane normal-aligned specimens with 30 vol% glass spheres were not able to be made because the geometry of the cell prevented complete photopolymerization. At 20 vol%, the average fracture toughness varied from 1.5 MPa $m^{1/2}$ for the in-plane normal-aligned specimens to 2.6 MPa $m^{1/2}$ for the

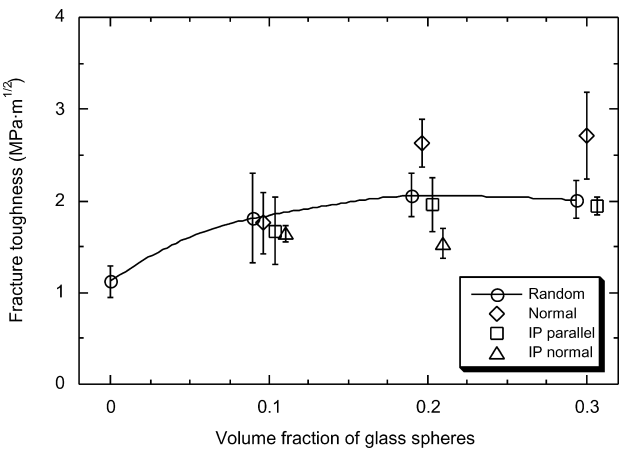

Fig. 4. The fracture toughness as a function of particle concentration and arrangement. Data obtained for the volume fractions of 0, 0.1, 0.2, and 0.3 were shifted horizontally from these abscissa values to prevent overlap. The error bars are for ±1 standard deviation. The curve connecting the data from randomly arranged glass spheres is meant only as a guide to this data.

normal-aligned specimens; the average fracture toughness of the random and in-plane parallel-aligned specimens at this particle concentration were 2.1 and 2.0 MPa $m^{1/2}$, respectively.

The fracture toughness results were also converted to fracture energy, G_{ic}. For the non-aligned specimens, Eq. (2) was used. For the aligned specimens, the fracture energy was calculated using orthotropic fracture mechanics [27] because alignment caused the elastic behavior to become anisotropic. The flexural modulus is shown plotted against particle concentration in Fig. 5. The flexural modulus with the particle strings along the beam axis was ca. 1.2 times greater than when the strings were transverse to the beam axis at all particle concentrations.

The fracture energy and its dependence on particle concentration and arrangement is shown in Fig. 6. The fracture energy of the neat resin was 340 J/m^2. For specimens with non-aligned particles, the average fracture energy appeared to reach a maximum of ca. 2.3 times that of the resin at a particle concentration between 10 and 20 vol%. Differences in fracture energy resulting from particle alignment were similar to those observed for fracture toughness. At 10 vol% glass spheres, all particle arrangements had about the same fracture energy. At 20 and 30 vol%, the normal-aligned specimens exhibited higher fracture energy than the non-aligned composites, the in-plane parallel-aligned specimens had about the same fracture energy as the non-aligned composites, and at 20 vol%, the in-plane normal-aligned specimens displayed lower fracture energy than the non-aligned composites. At 20 vol%, the average fracture energy ranged from 550 J/m^2 for the in-plane normal-aligned specimens to 1500 J/m^2 for the normal-aligned specimens; the average fracture energy of the random and in-plane parallel-aligned specimens at this particle concentration displayed similar values of 800 and 910 J/m^2, respectively.

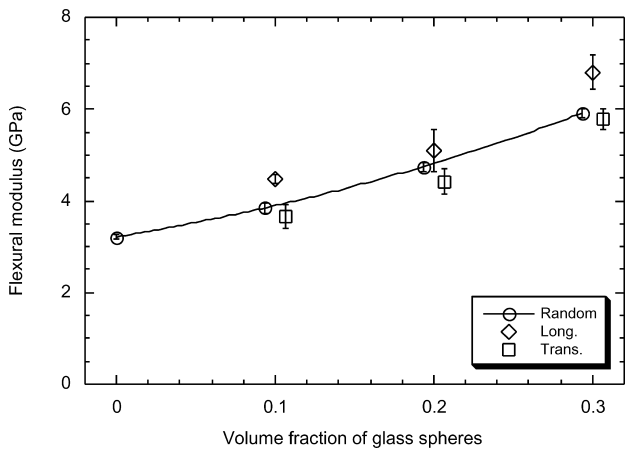

Fig. 5. The flexural modulus as a function of particle concentration and arrangement. Data has again been shifted horizontally to prevent overlap; the error bars are for ± 1 standard deviation; and the curve serves only as a guide to the data from randomly arranged glass spheres.

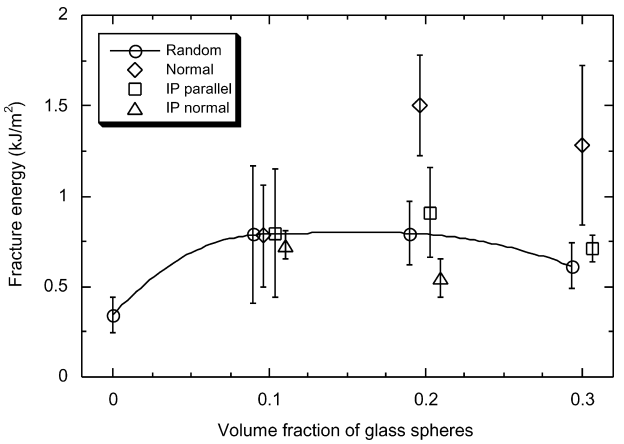

Fig. 6. The fracture energy as a function of particle concentration and arrangement. Data has again been shifted horizontally to prevent overlap; the error bars are for ± 1 standard deviation; and the curve serves only as a guide to the data from randomly arranged glass spheres.

3.3. Onset of inelastic deformation

The stress at the onset of inelastic behavior, σ_{ii}, was obtained from the flexure of unnotched bars, using a 0.1% offset strain criterion. σ_{ii} is plotted against particle concentration in Fig. 7. Optical microscopy of loaded flexural specimens revealed significant particle-matrix debonding occurred along the tensile side of the specimen as the stress approached σ_{ii}.

For the neat resin, the onset of inelastic deformation occurred at 110 MPa. (The yield stress measured in compression was 130 MPa.) For specimens with randomly arranged particles, the onset of inelastic deformation occurred at ca. 100 MPa for 10 and 20 vol%; for 30 vol%, brittle fracture occurred just before reaching the offset criterion, and σ_{ii} was estimated to be ca. 120 MPa, by extrapolating the stress–strain curve to the offset line. (Estimates obtained by extrapolation are enclosed within

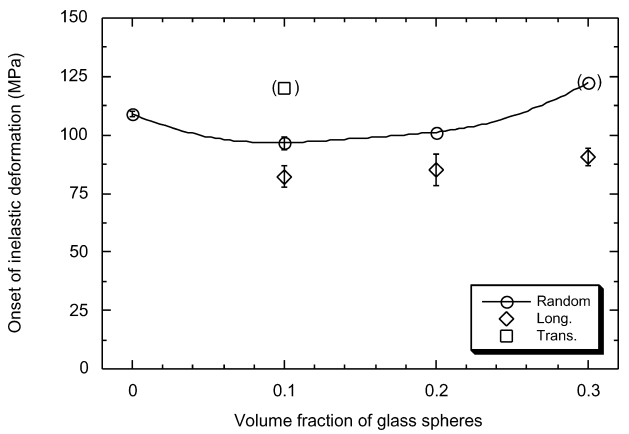

Fig. 7. The onset of inelastic deformation as a function of particle concentration and arrangement, measured in flexure, from 0.1% offset. Error bars are for ± 1 standard deviation, and the curve serves only as a guide to the data from randomly arranged glass spheres. Data in parentheses were not measured but were estimated by extrapolation.

parentheses in Fig. 7.) With the particle strings aligned along the specimen axis, inelastic deformation began ca. 20 MPa below that of the non-aligned composites for all particle concentrations. With the particles aligned transversely to the specimen axis, the onset of inelastic deformation occurred at a higher stress than with the non-aligned composites for 10 vol%; but the 20 and 30 vol% specimens failed with little deviation from linearity, which prevented our obtaining even estimates of σ_{ii}.

4. Discussion

For specimens with non-aligned particles, the fracture toughness increased with particle concentration and reached a plateau above about 20 vol% (Fig. 4); the fracture energy also increased and appeared to reach a broad maximum between 10 and 20 vol% (Fig. 6). This behavior is similar to that of previous studies on glassy polymers filled with rigid particles [1,7,9–13]. At 10 vol%, all particle arrangements displayed about the same toughness. At 20 and 30 vol%, the normal-aligned specimens were tougher than those without alignment, the in-plane parallel-aligned specimens had about the same toughness as without alignment, and at 20 vol%, the in-plane normal-aligned specimens were less tough.

This behavior can be compared with predictions from on- and off-fracture plane processes.

4.1. On-fracture plane processes: crack pinning and bowing

According to the crack bowing theory, toughening arises from the particles impeding crack growth. The advancing crack is assumed to be pinned by the particles, causing the crack front to bow out between particles. Then after the crack propagates a distance of about one particle diameter, the front breaks free and is able to return to a line shape. The two parameters controlling toughening are the lateral separation between particles at the crack front and the distance the crack propagates along the particles before breaking free. The latter will be referred to as the critical propagation distance. The average particle separation may be derived from particle concentration and diameter, as described below. The critical propagation distance was set equal to the particle diameter by Evans [15], though it was treated as an adjustable parameter by Green [16]. Other things being equal, crack bowing theory predicts increased toughness as the separation between particles decreases and as the critical propagation distance increases.

The separation between particles or strings, $\bar{s}$, is related to the number of particles or strings that are intersected by a line of unit length, N_L. With $\bar{s}$ being the average line length in the matrix between particles and letting $\bar{l}$ denote the average line length residing in each particle, N_L becomes

$$N_L = (\bar{s} + \bar{l})^{-1} \tag{5}$$

For composites without long-range order, the fraction of the unit line that is within the particles equals the volume fraction of particles [28]

$$V_f = N_V V_p = N_L \bar{l} = \bar{l}(\bar{s} + \bar{l})^{-1} \tag{6}$$

where N_V is the number of particles per unit volume and V_p the average particle volume.

Consider now a cube of unit dimensions containing N_V randomly distributed spherical particles of uniform size. Periodic boundary conditions are assumed in which particles protruding from one surface reenter on the opposite surface. If a line is drawn through the unit cube parallel to one of the edges, the number of particles intersected by the line is

$$N_L = N_V p = N_V \pi r_p^2 \tag{7}$$

where p is the probability that a particle will be intersected by the line and r_p the particle radius [29]. (The number of particles intersected by a line is the same as the number of particle centers that would be found within a tube centered on the line and having radius r_p.) Now consider the particles within the unit cube to be arranged in strings of n particles aligned parallel to one of the cube edges. Assume the particles to touch at their poles along the length of the strings, and assume further that the centers of the strings are randomly distributed throughout the cube. The average number of strings intersected by the unit line when perpendicular to the strings is

$$N^*_{L,\perp} = N^*_V p^*_\perp = \left(\frac{N_V}{n}\right)(n\pi r_p^2) = N_L \tag{8}$$

where N^*_V is the number of strings within the unit cube and $p^*_\perp$ the probability that a string perpendicular to the line will be intersected. (The asterisk is used to denote variables that relate to strings rather than individual particles.) The number of strings intersected per unit length by a line parallel to the strings is

$$N^*_{L,\parallel} = N^*_V p^*_\parallel = \left(\frac{N_V}{n}\right)\pi r_p^2 = \frac{N_L}{n} \tag{9}$$

where $p^*_\parallel$ is the probability that a string parallel to the line will be intersected.

To compute the average particle separation for randomly arranged particles, we first note that the average intersected particle length obtained from Eqs. (6) and (7) and $V_p = (4/3)\pi r_p^3$ is

$$\bar{l} = \frac{2}{3} d_p \tag{10}$$

where d_p is the particle diameter ($2r_p$). Then, from Eqs. (6) and (10)

$$\bar{s} = \frac{2d_p(1 - V_f)}{3V_f} \tag{11}$$

This is the particle separation used in prior investigations of rigid-particle toughening [2,6,7,9,10,20].

For strings intersected by a line perpendicular to their length, the average intersected length, $\bar{l}^*_\perp$, is the same as that of randomly arranged particles because the line intersects each string at a single particle; therefore, the separation between strings, $\bar{s}^*_\perp$, obtained from Eq. (5), equals $\bar{s}$ because $N^*_L = N_L$ and $\bar{l}^*_\perp = \bar{l}$. For strings intersected by a line parallel to their length, the average intersected string length, $\bar{l}^*_\parallel$, is equal to the distance between the centers of the outer particles in the string plus the average intersected length of a single particle

$$\bar{l}^*_\parallel = d_p(n-1) + \bar{l} = \frac{d_p(3n-1)}{3} \tag{12}$$

This adjusts for the small gaps between particles within the strings when the string is intersected off-center, which on average are of length $d_p/3$. The average separation between strings intersected by a line parallel to their length obtained from Eqs. (5), (6), (9), and (12) is

$$\bar{s}^*_\parallel = \frac{d_p(2n - 3nV_f + V_f)}{3V_f} \tag{13}$$

The critical propagation distance is assumed to be equal to the average length of the obstacle along the direction of crack propagation. For the non-aligned composites, the average critical propagation distance is $\bar{l}$. For the aligned composites, the average critical propagation distance is $\bar{l}^*_\perp$ when the crack propagates perpendicular to the strings and $\bar{l}^*_\parallel$ when the crack propagates parallel to the strings. $\bar{l}^*_\perp$ is generally an average particle diameter, but $\bar{l}^*_\parallel$ is generally the length of the average string.

The predictions of the crack bowing theory can now be stated. For the normal-aligned composites, crack bowing theory predicts the same toughness as for the non-aligned composites. This is because the separation between particles or strings and the critical propagation distance is the same for both particle arrangements ($\bar{s}^*_\perp = \bar{s}$ and $\bar{l}^*_\perp = \bar{l}$). For the in-plane parallel-aligned composites, crack bowing theory predicts greater toughness than for the non-aligned composites. This occurs because the critical propagation distance is greater for this particle arrangement than for non-aligned composites ($\bar{l}^*_\parallel > \bar{l}$) and the lateral separation between particles or strings is the same ($\bar{s}^*_\perp = \bar{s}$). For the in-plane normal-alignment, crack bowing theory predicts the toughness to be either less than or greater than for the non-aligned composites, because crack bowing may occur either only between strings or between particles within the strings. If bowing occurs between strings, the toughness is predicted to be less than the non-aligned composites because the spacing between the strings ($\bar{s}^*_\parallel$) is greater than that of randomly arranged particles ($\bar{s}$) and the critical propagation distance is the same as the non-aligned specimens ($\bar{l}^*_\perp = \bar{l}$). If bowing occurs between particles within the strings, the toughness is predicted to be greater than the non-aligned composites because the average separation between particles within the strings ($d_p/3$) is less than that of the non-aligned specimens ($\bar{s}$) over the range of particle concentration investigated, and the critical propagation distance is the same as the non-aligned specimens ($\bar{l}^*_\perp = \bar{l}$).

These predictions from crack bowing theory can be compared with the fracture results in Fig. 4. For normal-aligned composites, crack bowing predicts the fracture toughness to be the same as for non-aligned composites, but the fracture toughnesses of the normal-aligned composites at 20 and 30 vol% were found to be greater. For in-plane parallel-alignment, crack bowing predicts greater toughness than for non-aligned composites, but the fracture toughnesses of the two were about the same over the range of particle concentration investigated. For in-plane normal-alignment, crack bowing predicts lower toughness than the non-aligned composites if bowing is between the strings and greater toughness if bowing is between particles within the strings. The fracture toughness of the in-plane normal-aligned composites was about the same as the non-aligned specimens at 10 vol% and less than at 20 vol%. These disparities suggest that the on-fracture plane processes of crack pinning and bowing was not the operative toughening mechanism in this system.

4.2. Off-fracture plane processes: process zone size

Off-fracture plane toughening processes occur within a process zone around the crack tip during fracture. The processes occurring within the zone may include particle-matrix debonding, matrix yielding, and matrix micro-cracking. The role of off-fracture plane processes can be examined by comparing the observed and the calculated dimensions of the process zone.

Typical inelastic processes around a wedge-loaded crack tip can be seen in Fig. 8, which shows a thin section (ca. 1 mm thick) cut from a 10 vol%, normal-aligned specimen,

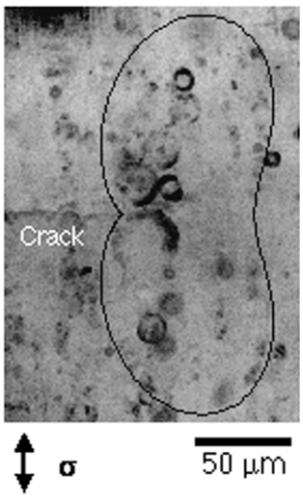

Fig. 8. Particle-matrix debonding around the crack tip in a thin section under load of a 10 vol%, normal-aligned specimen (ca. 1 mm thick). The calculated process-zone boundary for this specimen is superimposed on the micrograph.

here viewed with transmitted light. The crack is the faint, horizontal line on the left of the micrograph, and the crack tip is in the center of the micrograph, where it intersects a particulate string. The size of the process zone is the width of the region about the crack tip over which inelastic processes can be observed. Particle-matrix debonding was the most obvious inelastic process. This is seen in Fig. 8 as dark crescents around the poles of the particles. Similar debonding was observed in flexural specimens loaded above σ_{ii}. Process zone measurements were conducted for the non-aligned, normal-aligned, and in-plane parallel-aligned specimens with 10 and 20 vol% glass beads. Limitations of the technique prevented observations of specimens with 30 vol% glass beads or in-plane normal-alignment. For non-aligned specimens, the process zone extended more than 100 μm away from the fracture plane, which agrees with observations reported for other, similar systems [17,20].

The process zone boundary has been calculated by comparing the local stress state around the crack tip with the stress at which inelastic deformation occurs, σ_{ii}. The calculations assume that debonding arises from the largest normal stress acting across the particle-matrix interface. For aligned specimens, σ_{ii} was only measured with the particle strings along and transverse to the specimen axis. For this reason, the calculations assume that the process zone boundary is determined by the normal stresses either parallel or perpendicular to the strings. These directions may be defined by a Cartesian coordinate system with the crack tip at the origin and x along the crack propagation direction, y normal to the fracture plane, and z parallel to the unbowed crack front. The normal stresses along these directions have been approximated under plane-strain conditions at fracture using [26]

$$\sigma_{xx} = \frac{K_{Ic}}{\sqrt{2\pi r}}\cos\frac{\theta}{2}\left[1 - \sin\frac{\theta}{2}\sin\frac{3\theta}{2}\right] \tag{14}$$

$$\sigma_{yy} = \frac{K_{Ic}}{\sqrt{2\pi r}}\cos\frac{\theta}{2}\left[1 + \sin\frac{\theta}{2}\sin\frac{3\theta}{2}\right]$$

$$\sigma_{zz} = \nu(\sigma_{xx} + \sigma_{yy})$$

where θ and r describe the polar coordinates of a point in the xy plane with respect to the crack tip. The boundary of the process zone has been calculated as a function of θ by setting each normal stress equal to σ_{ii} and solving for r. This leads to three contours (i.e. $\sigma_{ii} = \sigma_{xx}$, $\sigma_{ii} = \sigma_{yy}$, and $\sigma_{ii} = \sigma_{zz}$), and the largest at each angle is assumed to be the process zone boundary. Values for K_{Ic} and σ_{ii} from Figs. 4 and 7 were used for the process zone calculations. For transversely aligned specimens, σ_{ii} was assumed to be 120 MPa, the estimated value for 10 vol%, for all particle concentrations.

Calculated process zone boundaries are shown in Fig. 9 for the various particle arrangements at 20 vol%. The calculated process zone boundary for a 10 vol%, normal-aligned specimen was also superimposed on the micrograph in Fig. 8. For most, the boundary was determined by the stress along the y-direction (i.e. the contour defined by $\sigma_{ii} = \sigma_{yy}$) and was kidney-bean shaped. The one exception was for in-plane parallel-alignment, for which the boundary arose from a combination of σ_{xx} and σ_{yy}. The stress along the x-direction extended the process zone ahead of the crack tip for this particle arrangement. The different shapes and sizes of the contours in Fig. 9 arise from the different onsets of inelastic strain. The onset was noticeably lower when the stress was along the aligned strings, expanding the process zones accordingly: upward and downward for normal-aligned and toward the right for in-plane parallel-aligned specimens.

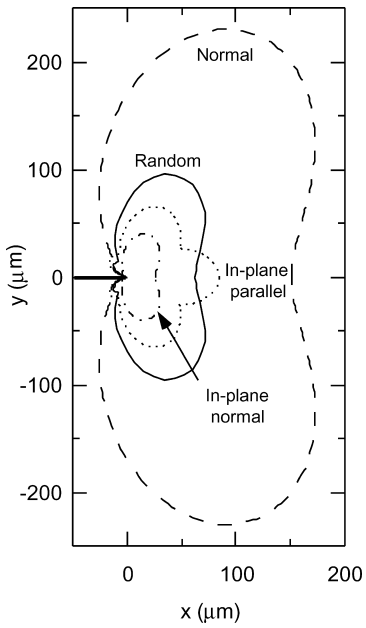

Fig. 9. Comparison of the process zone boundaries calculated for randomly arranged and aligned composites at a particle concentration of 20 vol%.

Comparisons of the observed and calculated process zone heights, h_p, and widths, w_p, are given in Fig. 10. The process zone height and width are the distances the process zone extends away from the crack tip in the y and x-directions, respectively. The open symbols in Fig. 10 are for particle concentrations of 10 vol%; the filled symbols are for 20 vol%. The observed and calculated values of process zone size are about the same for the particle concentrations and arrangements investigated. Also, the width measurements for the in-plane parallel-aligned specimens confirm that the process zone does indeed extend ahead of the crack tip in this particle arrangement.

As a further illustration of the role of the process zone size in rigid-particle toughening, the calculated process zone height, h_p, is plotted against particle concentration in Fig. 11 for all particle arrangements. For non-aligned specimens, h_p is predicted to increase with particle concentration, reaching a maximum of ca. 100 μm around 20 vol%. Similar trends in process zone size with particle concentration have been calculated by Young and Beaumont for a silica-filled epoxy [7]. For normal-aligned

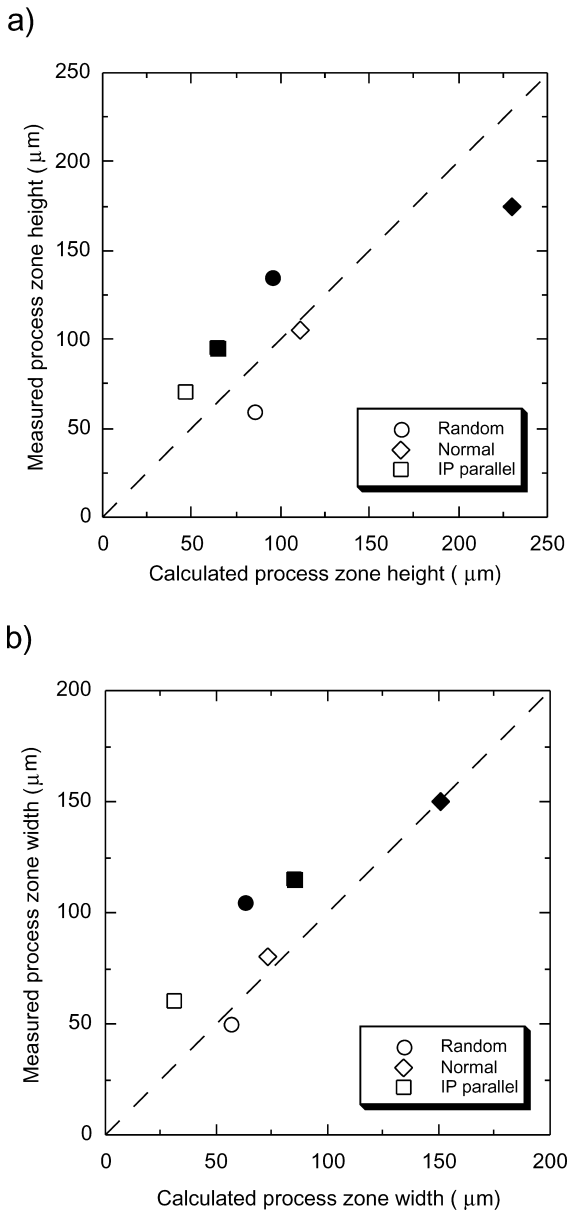

Fig. 10. Comparison of measured and calculated process zone (a) heights and (b) widths. Open symbols are for 10 vol% particle concentrations; filled symbols are for 20 vol% concentration.

specimens, the height of the process zone is predicted to be larger than the non-aligned specimens, especially at 20 and 30 vol%. For in-plane parallel-aligned specimens, the process zone height is predicted to be smaller than the non-aligned specimens at 10 and 20 vol% but about the same at 30 vol%. For in-plane normal-aligned specimens, the height of the process zone is predicted to be smaller than the non-aligned specimens at 10 and 20 vol%. Of particular note is the overall similarity in trends for h_p with particle concentration and alignment in Fig. 11 and those for fracture energy in Fig. 6, except for the greater variation in h_p at 10 vol%.

The process zones created by the initiating and growing crack for the present system were seen in the above to be

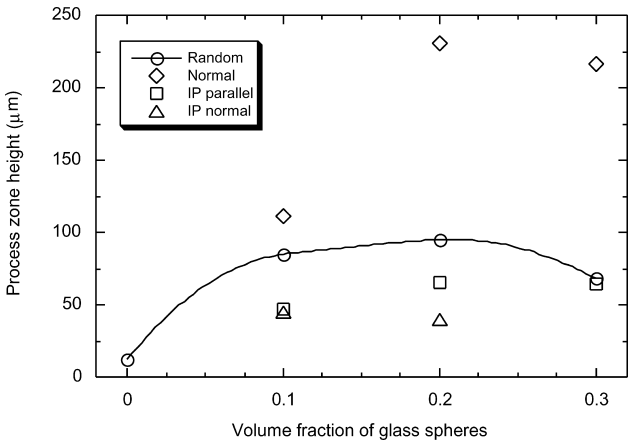

Fig. 11. Calculated process zone heights versus particle concentration for the different particle arrangements. The line connecting the data for randomly arranged particles is included only as a guide.

correlated with fracture behavior. In Section 4.3 we examine whether or not the various energy absorbing processes in the off-fracture plane process zone can quantitatively account for the rigid-particle toughening.

4.3. Off-fracture plane processes: estimation of fracture energy

The extra energy absorbed during fracture upon addition of rigid particles is assumed for the present to arise only from contributions off the fracture plane. These processes must also make up for the reduced contribution from matrix fracture when particles are present because the matrix fracture area is less. The main off-fracture plane processes considered are particle-matrix debonding and inelastic matrix deformation. Particle-matrix debonding is observed around the crack tip of wedge-loaded specimens (Fig. 8). The concomitant inelastic deformation of the matrix, which leaves gaps around the debonded particles, has allowed the debonding to become visible. Since both processes relate to debonding, the total contribution from off-fracture plane processes is assumed to be proportional to the number of debonded particle-matrix interfaces. Processes observed around the crack tip match those reported for other filled thermosets [11,12,17,18]. A schematic representation of the off-fracture plane processes associated with particle-matrix debonding is shown in Fig. 12.

The contribution from particle-matrix debonding arises from the energy needed to break the particle-matrix bond. The fracture energy of the interface has been estimated to be [30]

$$G_{ic,i} = \frac{3\sigma_d^2 r_p}{4\pi E_m} \tag{15}$$

where E_m is the modulus of the matrix (3.2 GPa), and σ_d the stress needed to initiate debonding. Setting σ_d equal to the stress for the onset of inelastic deformation, the interfacial fracture energy is estimated to be slightly less than 10 J/m^2,

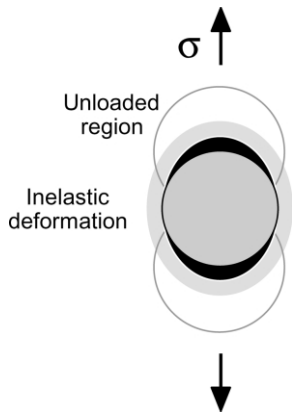

Fig. 12. Schematic of the processes associated with particle-matrix debonding.

which is similar to what Andrews et al. reported for an epoxy-glass interface in the absence of moisture [31].

The contribution from inelastic matrix deformation assumes that the deformation is localized around the debonded particle and that the inelastic strain is large enough to leave a gap upon unloading. The inelastic matrix deformation is assumed to occur within an ellipsoidal shell around the debonded particle (Fig. 12). For the gap to remain open after unloading, the inelastic strain must also overcome the shrinkage strain arising from the curing of the matrix. The shrinkage stress generated while cooling from the glass transition temperature, which is taken to be the cure temperature, is given by [32]

$$\sigma_r = -2\sigma_t = \frac{-(\alpha_m - \alpha_f)\Delta T}{(1+\nu_m)/E_m + (1-2\nu_f)/E_f} \tag{16}$$

where σ_r and σ_t are the radial and tangential stresses, ΔT the difference between the cure and ambient temperatures (ca. 125 °C), and α the coefficient of thermal expansion ($\alpha_m = 10^{-4}$ and $\alpha_f = 3\times10^{-6}\ K^{-1}$). This gives radial and tangential stresses of -54 and 27 MPa, respectively, which correspond with a compressive radial strain of 2.3%. Therefore, for gaps to remain open after unloading, the inelastic strain in the matrix must be greater than ca. 3%.

The total contribution from off-fracture plane processes depends on the number of particles that debond, which depends on the process zone height and particle concentration. The number of particles within the process zone per unit area, N_{PZ}, is the product of the span of the process zone, both above and below the fracture plane, and the volume fraction of particles divided by the particle volume

$$N_{PZ} = \frac{3h_p V_f}{2\pi r_p^3} \tag{17}$$

However, observation has shown that not all particle-matrix interfaces within the process zone debond. First, debonding appeared to depend on particle size: particles with diameters less than ca. 10 μm were rarely observed to debond. This effect of particle size agrees with the process zone observations by Lee and Yee [18] and the predictions by Gent [30]. Second, debonding appeared to depend on the proximity of nearby particles and decreased with increasing particle concentration. This was especially noticeable when the strings were loaded along their length: only about one-half of the interfaces that could debond did. This seemed to arise from localized unloading of the matrix around the debonded particles (Fig. 12); portions of nearby particles that fell within these unloaded regions were unlikely to debond. The extent of debonding observed with wedge-loaded fracture specimens may be summarized by

$$f_d(V_f) = f_{d,max} - (f_{d,max} - f_{d,min})\frac{V_f}{V_{f,max}} \tag{18}$$

where $f_d(V_f)$ is the fraction of debonded interfaces, $f_{d,max}$, and $f_{d,min}$ the upper and lower limits on the observed fraction of debonded interfaces, and $V_{f,max}$ the upper limit for particle volume fraction, 74% for close-packed spheres. For random and both in-plane alignments, the upper limit, $f_{d,max}$, was ca. 80% because about 20% of the particles were smaller than 10 μm in diameter. For normal-aligned specimens, $f_{d,max}$ was observed to be about 60%. The lower limit for $f_{d,min}$ was about 40%, or one-half the maximum value, because only about half of the particle-matrix interfaces appeared to debond within strings loaded along their length.

The sum of the several contributions described above allows the composite fracture energy to be estimated. The matrix contribution is proportional to the area fraction of the matrix within the fracture plane, and the off-fracture plane contribution is proportional to the number of particles within the process zone (Eq. (17)) times the fraction that debond (Eq. (18)). The contribution from particle-matrix debonding is $G_{ic,i}$ times the surface area of the particle, and the contribution from inelastic matrix deformation is the volume deformed around each particle, V_{in}, times the work per unit volume to deform the matrix, W_{in}. Together these give

$$G_{ic,c} = (1-V_f)G_{ic,m} + \frac{3h_p V_f f_d(V_f)}{2\pi r_p^3}(4\pi r_p^2 G_{ic,i} + V_{in}W_{in}) \tag{19}$$

where the subscripts c, m, and i refer to the composite, matrix, and interfacial bond. For calculating the composite fracture energy, the matrix fracture energy is 340 J/m^2, the average particle radius is 10 μm (diameter, 20 μm), the height of the process zone is given in Fig. 11, and $G_{ic,i}$ is 10 J/m^2. The inelastic deformation is assumed to occur within a spherical shell around the debonded particle with a thickness of $r_p/4$. This is the volume V_{in}, and it is equal to roughly twice that of the particle. The work needed to inelastically deform the matrix, W_{in}, has been estimated to be ca. 10 MJ/m^3 from the area underneath a stress–strain curve of the resin using an inelastic strain of 5%.

In the above analysis, the inelastic deformation of the matrix around debonded particles represents the largest contribution to the fracture energy, ca. 50%. Fracture of the

matrix provides ca. 40% of the composite fracture energy, and particle-matrix debonding accounts for less than 10% of the composite fracture energy.

The fracture energies were calculated from the above analysis together with the particle concentrations and arrangements. A comparison of the calculated and measured fracture energies is shown in Fig. 13. The open symbols in Fig. 13 are for measured values, and the filled symbols are for calculated values. Although the calculated fracture energy underestimates the measured values at 10 vol% and overestimate those at 30 vol%, especially for normal-aligned specimens, the two sets of values generally agree. The calculations predict the following. For specimens with randomly arranged particles, the fracture energy is increased by a factor of about 2.5, reaching a maximum around 20 vol% glass spheres. At 10 vol%, the fracture energies of the non-aligned and normal-aligned specimens are slightly greater than the two in-plane-alignments. At 20 vol%, the fracture energy of the normal-aligned specimens is significantly greater than the non-aligned composites, and those of both in-plane-alignments are less than the non-aligned composites. At 30 vol%, the fracture energy for normal-aligned specimens is significantly greater than for non-aligned composites, and that for in-plane parallel-aligned specimens is about the same as for non-aligned.

4.4. Relative contributions of on- and off-fracture plane processes

The relative contributions of on- and off-fracture plane processes may be addressed by considering how the comparison of measured and calculated fracture energies in Fig. 13 would be altered by the inclusion of crack pinning and bowing. (Only off-fracture plane processes were considered for the calculated (filled) points in Fig. 13.) The following calculations were based on the approach of

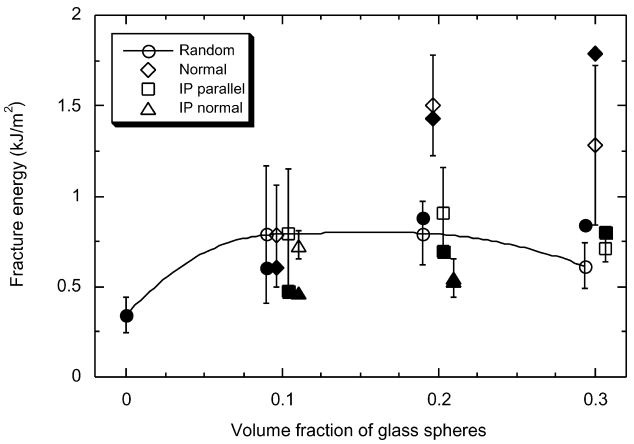

Fig. 13. Comparison of measured and calculated fracture energies for the different particle concentrations and arrangements. Open symbols are experimental; filled symbols are calculated. Data has again been shifted horizontally to prevent overlap. The error bars are for ±1 standard deviation. The curve for the randomly arranged glass spheres refers to the experimental data.

Evans [15]. Bowed cracks were assumed to be semi-circular and to interact with one another, and Eqs. (10)–(13) were used to describe the average critical propagation distance and average separation between particles or strings.

The addition of the fracture energies predicted by crack bowing to those for off-fracture plane processes would raise all of the calculated (filled) points in Fig. 13. This would move the calculated and measured points for the 10 vol% data closer together, but it would move the calculated and measured points for the 30 vol% data further apart and have a mixed effect for the 20 vol% data. A general raising of the calculated fracture energies, however, is not a definitive test of a possible role for crack bowing. A more critical test is the relative change of the calculated fracture energies for each volume fraction. As noted in Section 4.1, for a given volume fracture of glass spheres, crack bowing predicts the fracture energy of normal aligned specimens to be the same as non-aligned, the in-plane normal specimens to be greater than non-aligned, and the in-plane parallel to be either greater than or less than non-aligned specimens. The calculated fracture energies for 10 vol% would be helped by these differences if both in-plane specimens had greater fracture energies than the non-aligned (and normal-aligned) specimens. In Fig. 13, all filled points for 10 vol% would move up, with the points for the in-plane specimens moving up faster than those for normal-aligned and non-aligned. For 20 and 30 vol%, however, the inclusion of crack bowing results in little or no improvement, if not a worsening, of the calculated fracture energies. The calculated fracture energy (without crack bowing) for 20 vol% in-plane normal is essentially the same as that measured (Fig. 13), and those calculated (without crack bowing) for the random specimens (both 20 and 30 vol%) already exceed those measured. The fracture energies calculated without crack bowing for normal-aligned and in-plane parallel are both smaller than measured for 20 vol% and both greater than measured for 30 vol%. Thus, there is little need to assume any role for crack bowing. On the other hand, the scatter in the measured fracture energies is such that a minor role for crack bowing (a few percent of the predicted toughening effect) cannot be dismissed.

4.5. Significance for other systems

For the present system, off-fracture plane processes were able to account for most, if not all, of the rigid-particle toughening, and crack pinning and bowing accounted for little or none. The significance of this for other systems may be addressed by comparing the materials and fracture behavior of the present study with those of previous studies. The materials are similar. Glassy polymers that yield in compression but are brittle in tension have been used as the matrix in nearly all studies, including the present. The matrices previously studied include epoxy resins [2–4,6–12,18–20,22], unsaturated polyester resins [4,5,21], methacrylate resins [1,23], and polystyrene [13]. Also,

glass beads have been extensively investigated [4–6,9,10,12,13,18–20,22], and the use of beads without any surface treatments is common [4–6,9,12,18,20].

The interfacial strength between the matrix and glass spheres is also expected to be similar. A strong interfacial bond requires intimate contact between the two surfaces, which usually means that the liquid matrix resin must completely wet the substrate before polymerization. This is assisted by reducing the liquid resin viscosity by heating. For the present system, the particle–liquid resin mixture was heated to ca. 75 °C to release entrapped air, and this also furthered particle wetting. High adhesive bond strength between a polymer resin and a mineral filler is conventionally thought to require a silane coupling agent on the filler. But many adhesive studies have shown little difference between with and without silane coupling agents when the specimens are dry, as long as the liquid matrix resin has wetted the substrate. The main enhancement by coupling agents has been found in the presence of moisture. Thus, where surface treatments have been applied, the magnitude of the toughening was little altered [1,4,5,8,21–23,33], and the bond strength in the present system is believed to be comparable to that in previous studies that showed rigid-particle toughening.

The fracture behavior of the systems studied has also been similar. For specimens of the present study without alignment, the fracture toughness increased with particle concentration, before leveling off above ca. 20 vol% (Fig. 4), and the fracture energy increased with particle concentration, reaching a maximum between 10 and 20 vol% (Fig. 6). These agree with reported trends for fracture toughness [1,7–13,22,23] and fracture energy [1–13,21] for a wide variety of fillers and matrices. Other fillers investigated in the past include alumina [8], alumina trihydrate [2,3], calcite [21], dolomite [8], and silica [7]. For many, if not all, of these systems, the similarity of materials and fracture behavior suggests that rigid-particle toughening is arising from the same mechanisms. Thus, off-fracture plane processes would seem to be the main rigid-particle toughening mechanisms in these systems, and crack pinning and bowing is of little importance.

5. Conclusions

Differences in fracture behavior between random and aligned particulate composites were used to evaluate existing interpretations for rigid-particle toughening of glassy polymers. Comparing predictions from these interpretations with fracture results has shown that off-fracture plane processes, such as particle-matrix debonding and inelastic matrix deformation, are the main toughening mechanisms, and crack pinning and bowing contribute little, if any. Of the off-fracture plane processes observed, inelastic deformation of the matrix provided the greatest toughening, and particle-matrix debonding provided much less. Since the materials and fracture behavior of the present non-aligned composites are typical of those in previous studies of filled, glassy polymers, the findings for the present system are likely to be valid for these other systems as well.

References

[1] Rothon R. Particulate-filled polymer composites. Essex: Longman Scientific and Technical; 1995.
[2] Lange FF, Radford KC. J Mater Sci 1971;6:1197.
[3] Radford KC. J Mater Sci 1971;6:1286.
[4] Broutman LJ, Sahu S. Mater Sci Engng 1971;8:98.
[5] Hammond JC, Quayle DV. Proceedings of the Second International Conference on Yield, Deformation, and Fracture of Polymers. Cambridge; 1973.
[6] Mallick PK, Broutman LJ. Mater Sci Engng 1975;18:63.
[7] Young RJ, Beaumont PWR. J Mater Sci 1977;12:684.
[8] Moloney AC, Kausch HH, Stieger HR. J Mater Sci 1983;18:208.
[9] Spanoudakis J, Young RJ. J Mater Sci 1984;19:473.
[10] Kinloch AJ, Maxwell DL, Young RJ. J Mater Sci 1985;20:4169.
[11] Nakamura Y, Yamaguchi M, Okubo M, Matsumoto T. Polymer 1992;33:3415.
[12] Lee J, Yee AF. Polymer 2000;41:8363.
[13] Sanchez-Soto M, Gordillo A, Maspoch MLL, Velasco JI, Santana OO, Martinez AB. Polym Bull 2002;47:587.
[14] Lange FF. Philos Mag 1970;22:983.
[15] Evans AG. Philos Mag 1972;26:1327.
[16] Green DJ, Nicholson PS, Embury JD. J Mater Sci 1979;14:1657.
[17] Owen AB. J Mater Sci 1979;14:2521.
[18] Lee J, Yee AF. Polymer 2001;42:577.
[19] Evans AG, Williams S, Beaumont PWR. J Mater Sci 1985;20:3668.
[20] Lee J, Yee AF. Polymer 2001;42:589.
[21] Brown SK. Br Polym J 1980;24.
[22] Moloney AC, Kausch HH, Stieger HR. J Mater Sci 1984;19:1125.
[23] Davis DM, Waters NE. J Dent Res 1987;66:1128.
[24] Park C, Robertson RE. Mater Sci Engng 1998;257A:295.
[25] ASTM Standard Test Method for Plane-Strain Fracture Toughness of Metallic Materials; 1983; E399: 518–53.
[26] Broek D. Elementary engineering fracture mechanics. Dordrecht: Kluwer Academic; 1986.
[27] Tada H. Stress analysis of cracks handbook. Saint Louis: Paris Productions; 1985.
[28] Piggott MR, Leidner J. J Appl Polym Sci 1974;18:1619.
[29] Fullman RL. J Met 1953;197:447.
[30] Gent AN. J Mater Sci 1980;15:2884.
[31] Andrews EH, Pingsheng H, Vlachos C. Proc R Soc London 1982;381A:345.
[32] Selsing J. J Am Ceram Soc 1961;44:491.
[33] Spanoudakis J, Young RJ. J Mater Sci 1984;19:487.